

Chapter 2

SURFACE PLASMON POLARITONS AT METAL / INSULATOR INTERFACES

Surface plasmon polaritons are electromagnetic excitations propagating at the interface between a dielectric and a conductor, evanescently confined in the perpendicular direction. These electromagnetic surface waves arise via the coupling of the electromagnetic fields to oscillations of the conductor's electron plasma. Taking the wave equation as a starting point, this chapter describes the fundamentals of surface plasmon polaritons both at single, flat interfaces and in metal/dielectric multilayer structures. The surface excitations are characterized in terms of their dispersion and spatial profile, together with a detailed discussion of the quantification of field confinement. Applications of surface plasmon polaritons in waveguiding will be deferred to chapter 7.

2.1 The Wave Equation

In order to investigate the physical properties of surface plasmon polaritons (SPPs), we have to apply Maxwell's equations (1.1) to the flat interface between a conductor and a dielectric. To present this discussion most clearly, it is advantageous to cast the equations first in a general form applicable to the guiding of electromagnetic waves, the *wave equation*.

As we have seen in chapter 1, in the absence of external charge and current densities, the curl equations (1.1c, 1.1d) can be combined to yield

$$\nabla \times \nabla \times \mathbf{E} = -\mu_0 \frac{\partial^2 \mathbf{D}}{\partial t^2}. \quad (2.1)$$

Using the identities $\nabla \times \nabla \times \mathbf{E} \equiv \nabla(\nabla \cdot \mathbf{E}) - \nabla^2 \mathbf{E}$ as well as $\nabla \cdot (\varepsilon \mathbf{E}) \equiv \mathbf{E} \cdot \nabla \varepsilon + \varepsilon \nabla \cdot \mathbf{E}$, and remembering that due to the absence of external stimuli $\nabla \cdot \mathbf{D} = 0$, (2.1) can be rewritten as

$$\nabla \left(-\frac{1}{\varepsilon} \mathbf{E} \cdot \nabla \varepsilon \right) - \nabla^2 \mathbf{E} = -\mu_0 \varepsilon_0 \varepsilon \frac{\partial^2 \mathbf{E}}{\partial t^2}. \quad (2.2)$$

For negligible variation of the dielectric profile $\varepsilon = \varepsilon(\mathbf{r})$ over distances on the order of one optical wavelength, (2.2) simplifies to the central equation of electromagnetic wave theory,

$$\nabla^2 \mathbf{E} - \frac{\varepsilon}{c^2} \frac{\partial^2 \mathbf{E}}{\partial t^2} = 0. \quad (2.3)$$

Practically, this equation has to be solved separately in regions of constant ε , and the obtained solutions have to be matched using appropriate boundary conditions. To cast (2.3) in a form suitable for the description of confined propagating waves, we proceed in two steps. First, we assume in all generality a harmonic time dependence $\mathbf{E}(\mathbf{r}, t) = \mathbf{E}(\mathbf{r})e^{-i\omega t}$ of the electric field. Inserted into (2.3), this yields

$$\nabla^2 \mathbf{E} + k_0^2 \varepsilon \mathbf{E} = 0, \quad (2.4)$$

where $k_0 = \frac{\omega}{c}$ is the wave vector of the propagating wave in vacuum. Equation (2.4) is known as the *Helmholtz equation*.

Next, we have to define the propagation geometry. We assume for simplicity a one-dimensional problem, i.e. ε depends only on one spatial coordinate. Specifically, the waves propagate along the x-direction of a cartesian coordinate system, and show no spatial variation in the perpendicular, in-plane y-direction (see Fig. 2.1); therefore $\varepsilon = \varepsilon(z)$. Applied to electromagnetic surface problems, the plane $z = 0$ coincides with the interface sustaining the

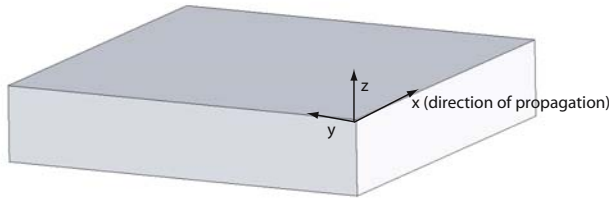


Figure 2.1. Definition of a planar waveguide geometry. The waves propagate along the x-direction in a cartesian coordinate system.

propagating waves, which can now be described as $\mathbf{E}(x, y, z) = \mathbf{E}(z)e^{i\beta x}$. The complex parameter $\beta = k_x$ is called the *propagation constant* of the traveling waves and corresponds to the component of the wave vector in the direction of propagation. Inserting this expression into (2.4) yields the desired form of the wave equation

$$\frac{\partial^2 \mathbf{E}(z)}{\partial z^2} + (k_0^2 \varepsilon - \beta^2) \mathbf{E} = 0. \quad (2.5)$$

Naturally, a similar equation exists for the magnetic field \mathbf{H} .

Equation (2.5) is the starting point for the general analysis of guided electromagnetic modes in waveguides, and an extended discussion of its properties and applications can be found in [Yariv, 1997] and similar treatments of photonics and optoelectronics. In order to use the wave equation for determining the spatial field profile and dispersion of propagating waves, we now need to find explicit expressions for the different field components of \mathbf{E} and \mathbf{H} . This can be achieved in a straightforward way using the curl equations (1.1c, 1.1d).

For harmonic time dependence ($\frac{\partial}{\partial t} = -i\omega$), we arrive at the following set of coupled equations

$$\frac{\partial E_z}{\partial y} - \frac{\partial E_y}{\partial z} = i\omega\mu_0 H_x \quad (2.6a)$$

$$\frac{\partial E_x}{\partial z} - \frac{\partial E_z}{\partial x} = i\omega\mu_0 H_y \quad (2.6b)$$

$$\frac{\partial E_y}{\partial x} - \frac{\partial E_x}{\partial y} = i\omega\mu_0 H_z \quad (2.6c)$$

$$\frac{\partial H_z}{\partial y} - \frac{\partial H_y}{\partial z} = -i\omega\varepsilon_0 \varepsilon E_x \quad (2.6d)$$

$$\frac{\partial H_x}{\partial z} - \frac{\partial H_z}{\partial x} = -i\omega\varepsilon_0 \varepsilon E_y \quad (2.6e)$$

$$\frac{\partial H_y}{\partial x} - \frac{\partial H_x}{\partial y} = -i\omega\varepsilon_0 \varepsilon E_z. \quad (2.6f)$$

For propagation along the x -direction ($\frac{\partial}{\partial x} = i\beta$) and homogeneity in the y -direction ($\frac{\partial}{\partial y} = 0$), this system of equation simplifies to

$$\frac{\partial E_y}{\partial z} = -i\omega\mu_0 H_x \quad (2.7a)$$

$$\frac{\partial E_x}{\partial z} - i\beta E_z = i\omega\mu_0 H_y \quad (2.7b)$$

$$i\beta E_y = i\omega\mu_0 H_z \quad (2.7c)$$

$$\frac{\partial H_y}{\partial z} = i\omega\varepsilon_0\varepsilon E_x \quad (2.7d)$$

$$\frac{\partial H_x}{\partial z} - i\beta H_z = -i\omega\varepsilon_0\varepsilon E_y \quad (2.7e)$$

$$i\beta H_y = -i\omega\varepsilon_0\varepsilon E_z. \quad (2.7f)$$

It can easily be shown that this system allows two sets of self-consistent solutions with different polarization properties of the propagating waves. The first set are the transverse magnetic (TM or p) modes, where only the field components E_x , E_z and H_y are nonzero, and the second set the transverse electric (TE or s) modes, with only H_x , H_z and E_y being nonzero.

For TM modes, the system of governing equations (2.7) reduces to

$$E_x = -i\frac{1}{\omega\varepsilon_0\varepsilon} \frac{\partial H_y}{\partial z} \quad (2.8a)$$

$$E_z = -\frac{\beta}{\omega\varepsilon_0\varepsilon} H_y, \quad (2.8b)$$

and the wave equation for TM modes is

$$\frac{\partial^2 H_y}{\partial z^2} + (k_0^2\varepsilon - \beta^2) H_y = 0. \quad (2.8c)$$

For TE modes the analogous set is

$$H_x = i\frac{1}{\omega\mu_0} \frac{\partial E_y}{\partial z} \quad (2.9a)$$

$$H_z = \frac{\beta}{\omega\mu_0} E_y, \quad (2.9b)$$

with the TE wave equation

$$\frac{\partial^2 E_y}{\partial z^2} + (k_0^2\varepsilon - \beta^2) E_y = 0. \quad (2.9c)$$

With these equations at our disposal, we are now in a position to embark on the description of surface plasmon polaritons.

2.2 Surface Plasmon Polaritons at a Single Interface

The most simple geometry sustaining SPPs is that of a single, flat interface (Fig. 2.2) between a dielectric, non-absorbing half space ($z > 0$) with positive real dielectric constant ε_2 and an adjacent conducting half space ($z < 0$) described via a dielectric function $\varepsilon_1(\omega)$. The requirement of metallic character implies that $\text{Re}[\varepsilon_1] < 0$. As shown in chapter 1, for metals this condition is fulfilled at frequencies below the bulk plasmon frequency ω_p . We want to look for propagating wave solutions confined to the interface, i.e. with evanescent decay in the perpendicular z -direction.

Let us first look at TM solutions. Using the equation set (2.8) in both half spaces yields

$$H_y(z) = A_2 e^{i\beta x} e^{-k_2 z} \quad (2.10a)$$

$$E_x(z) = i A_2 \frac{1}{\omega \varepsilon_0 \varepsilon_2} k_2 e^{i\beta x} e^{-k_2 z} \quad (2.10b)$$

$$E_z(z) = -A_1 \frac{\beta}{\omega \varepsilon_0 \varepsilon_2} e^{i\beta x} e^{-k_2 z} \quad (2.10c)$$

for $z > 0$ and

$$H_y(z) = A_1 e^{i\beta x} e^{k_1 z} \quad (2.11a)$$

$$E_x(z) = -i A_1 \frac{1}{\omega \varepsilon_0 \varepsilon_1} k_1 e^{i\beta x} e^{k_1 z} \quad (2.11b)$$

$$E_z(z) = -A_1 \frac{\beta}{\omega \varepsilon_0 \varepsilon_1} e^{i\beta x} e^{k_1 z} \quad (2.11c)$$

for $z < 0$. $k_i \equiv k_{z,i}$ ($i = 1, 2$) is the component of the wave vector perpendicular to the interface in the two media. Its reciprocal value, $\hat{z} = 1/|k_z|$, defines the evanescent decay length of the fields perpendicular to the interface,

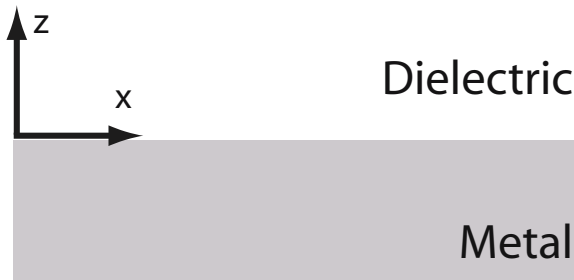


Figure 2.2. Geometry for SPP propagation at a single interface between a metal and a dielectric.

which quantifies the confinement of the wave. Continuity of H_y and $\varepsilon_i E_z$ at the interface requires that $A_1 = A_2$ and

$$\frac{k_2}{k_1} = -\frac{\varepsilon_2}{\varepsilon_1}. \quad (2.12)$$

Note that with our convention of the signs in the exponents in (2.10,2.11), confinement to the surface demands $\text{Re}[\varepsilon_1] < 0$ if $\varepsilon_2 > 0$ - the surface waves exist only at interfaces between materials with opposite signs of the real part of their dielectric permittivities, i.e. between a conductor and an insulator. The expression for H_y further has to fulfill the wave equation (2.8c), yielding

$$k_1^2 = \beta^2 - k_0^2 \varepsilon_1 \quad (2.13a)$$

$$k_2^2 = \beta^2 - k_0^2 \varepsilon_2. \quad (2.13b)$$

Combining this and (2.12) we arrive at the central result of this section, the dispersion relation of SPPs propagating at the interface between the two half spaces

$$\beta = k_0 \sqrt{\frac{\varepsilon_1 \varepsilon_2}{\varepsilon_1 + \varepsilon_2}}. \quad (2.14)$$

This expression is valid for both real and complex ε_1 , i.e. for conductors without and with attenuation.

Before discussing the properties of the dispersion relation (2.14) in more detail, we now briefly analyze the possibility of TE surface modes. Using (2.9), the respective expressions for the field components are

$$E_y(z) = A_2 e^{i\beta x} e^{-k_2 z} \quad (2.15a)$$

$$H_x(z) = -i A_2 \frac{1}{\omega \mu_0} k_2 e^{i\beta x} e^{-k_2 z} \quad (2.15b)$$

$$H_z(z) = A_2 \frac{\beta}{\omega \mu_0} e^{i\beta x} e^{-k_2 z} \quad (2.15c)$$

for $z > 0$ and

$$E_y(z) = A_1 e^{i\beta x} e^{k_1 z} \quad (2.16a)$$

$$H_x(z) = i A_1 \frac{1}{\omega \mu_0} k_1 e^{i\beta x} e^{k_1 z} \quad (2.16b)$$

$$H_z(z) = A_1 \frac{\beta}{\omega \mu_0} e^{i\beta x} e^{k_1 z} \quad (2.16c)$$

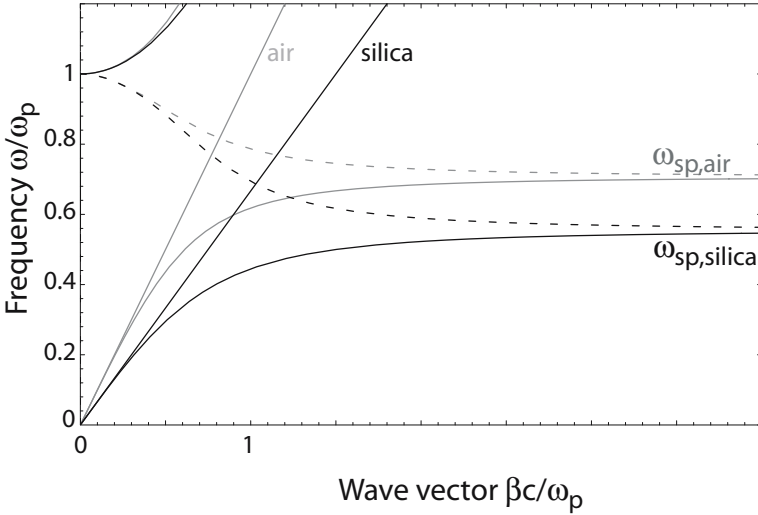


Figure 2.3. Dispersion relation of SPPs at the interface between a Drude metal with negligible collision frequency and air (gray curves) and silica (black curves).

for $z < 0$. Continuity of E_y and H_x at the interface leads to the condition

$$A_1(k_1 + k_2) = 0. \quad (2.17)$$

Since confinement to the surface requires $\text{Re}[k_1] > 0$ and $\text{Re}[k_2] > 0$, this condition is only fulfilled if $A_1 = 0$, so that also $A_2 = A_1 = 0$. Thus, no surface modes exist for TE polarization. *Surface plasmon polaritons only exist for TM polarization.*

We now want to examine the properties of SPPs by taking a closer look at their dispersion relation. Fig. 2.3 shows plots of (2.14) for a metal with negligible damping described by the real Drude dielectric function (1.22) for an air ($\epsilon_2 = 1$) and a fused silica ($\epsilon_2 = 2.25$) interface. In this plot, the frequency ω is normalized to the plasma frequency ω_p , and both the real (continuous curves) and the imaginary part (broken curves) of the wave vector β are shown. Due to their bound nature, the SPP excitations correspond to the part of the dispersion curves lying to the right of the respective light lines of air and silica. Thus, special phase-matching techniques such as grating or prism coupling are required for their excitation via three-dimensional beams, which will be discussed in chapter 3. Radiation into the metal occurs in the transparency regime $\omega > \omega_p$ as mentioned in chapter 1. Between the regime of the bound and radiative modes, a frequency gap region with purely imaginary β prohibiting propagation exists.

For small wave vectors corresponding to low (mid-infrared or lower) frequencies, the SPP propagation constant is close to k_0 at the light line, and the

waves extend over many wavelengths into the dielectric space. In this regime, SPPs therefore acquire the nature of a grazing-incidence light field, and are also known as *Sommerfeld-Zenneck waves* [Goubau, 1950].

In the opposite regime of large wave vectors, the frequency of the SPPs approaches the characteristic *surface plasmon frequency*

$$\omega_{\text{sp}} = \frac{\omega_p}{\sqrt{1 + \varepsilon_2}}, \quad (2.18)$$

as can be shown by inserting the free-electron dielectric function (1.20) into (2.14). In the limit of negligible damping of the conduction electron oscillation (implying $\text{Im}[\varepsilon_1(\omega)] = 0$), the wave vector β goes to infinity as the frequency approaches ω_{sp} , and the group velocity $v_g \rightarrow 0$. The mode thus acquires electrostatic character, and is known as the *surface plasmon*. It can indeed be obtained via a straightforward solution of the Laplace equation $\nabla^2\phi = 0$ for the single interface geometry of Fig. 2.2, where ϕ is the electric potential. A solution that is wavelike in the x-direction and exponentially decaying in the z-direction is given by

$$\phi(z) = A_2 e^{i\beta x} e^{-k_2 z} \quad (2.19)$$

for $z > 0$ and

$$\phi(z) = A_1 e^{i\beta x} e^{k_1 z} \quad (2.20)$$

for $z < 0$. $\nabla^2\phi = 0$ requires that $k_1 = k_2 = \beta$: the exponential decay lengths $|\hat{z}| = 1/k_z$ into the dielectric and into the metal are equal. Continuity of ϕ and $\varepsilon\partial\phi/\partial z$ ensure continuity of the tangential field components and the normal components of the dielectric displacement and require that $A_1 = A_2$ and additionally

$$\varepsilon_1(\omega) + \varepsilon_2 = 0. \quad (2.21)$$

For a metal described by a dielectric function of the form (1.22), this condition is fulfilled at ω_{sp} . Comparison of (2.21) and (2.14) show that the surface plasmon is indeed the limiting form of a SPP as $\beta \rightarrow \infty$.

The above discussions of Fig. 2.3 have assumed an ideal conductor with $\text{Im}[\varepsilon_1] = 0$. Excitations of the conduction electrons of real metals however suffer both from free-electron and interband damping. Therefore, $\varepsilon_1(\omega)$ is complex, and with it also the SPP propagation constant β . The traveling SPPs are damped with an energy attenuation length (also called propagation length) $L = (2\text{Im}[\beta])^{-1}$, typically between 10 and 100 μm in the visible regime, depending upon the metal/dielectric configuration in question.

Fig. 2.4 shows as an example the dispersion relation of SPPs propagating at a silver/air and silver/silica interface, with the dielectric function $\varepsilon_1(\omega)$ of silver

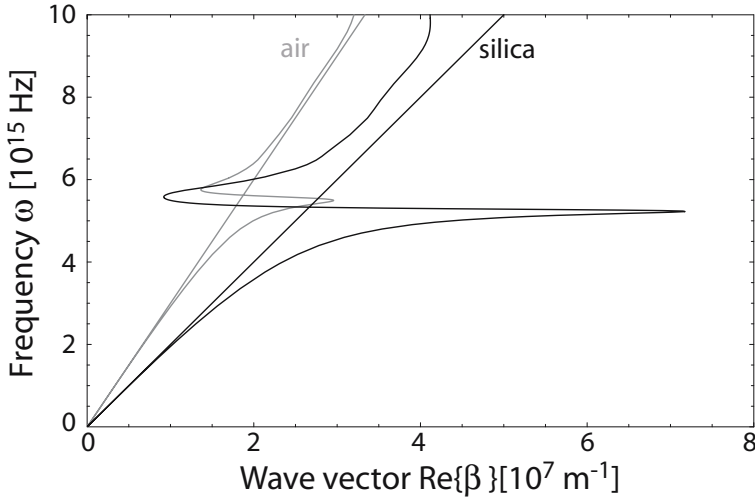


Figure 2.4. Dispersion relation of SPPs at a silver/air (gray curve) and silver/silica (black curve) interface. Due to the damping, the wave vector of the bound SPPs approaches a finite limit at the surface plasmon frequency.

taken from the data obtained by Johnson and Christy [Johnson and Christy, 1972]. Compared with the dispersion relation of completely undamped SPPs depicted in Fig. 2.3, it can be seen that the bound SPPs approach now a maximum, *finite* wave vector at the the surface plasmon frequency ω_{sp} of the system. This limitation puts a lower bound both on the wavelength $\lambda_{\text{sp}} = 2\pi/\text{Re}[\beta]$ of the surface plasmon and also on the amount of mode confinement perpendicular to the interface, since the SPP fields in the dielectric fall off as $e^{-|k_z||z|}$ with $k_z = \sqrt{\beta^2 - \varepsilon_2 \left(\frac{\omega}{c}\right)^2}$. Also, the *quasibound*, leaky part of the dispersion relation between ω_{sp} and ω_{p} is now allowed, in contrast to the case of an ideal conductor, where $\text{Re}[\beta] = 0$ in this regime (Fig. 2.3).

We finish this section by providing an example of the propagation length L and the energy confinement (quantified by \hat{z}) in the dielectric. As is evident from the dispersion relation, both show a strong dependence on frequency. SPPs at frequencies close to ω_{sp} exhibit large field confinement to the interface and a subsequent small propagation distance due to increased damping. Using the theoretical treatment outlined above, we see that SPPs at a silver/air interface at $\lambda_0 = 450$ nm for example have $L \approx 16 \mu\text{m}$ and $\hat{z} \approx 180$ nm. At $\lambda_0 \approx 1.5 \mu\text{m}$ however, $L \approx 1080 \mu\text{m}$ and $\hat{z} \approx 2.6 \mu\text{m}$. The better the confinement, the lower the propagation length. This characteristic trade-off between localization and loss is typical for plasmonics. We note that field-confinement below the diffraction limit of half the wavelength in the dielectric can be achieved close to ω_{sp} . In the metal itself, the fields fall off over distances

on the order of 20 nm over a wide frequency range spanning from the visible to the infrared.

2.3 Multilayer Systems

We now turn our attention to SPPs in multilayers consisting of alternating conducting and dielectric thin films. In such a system, each single interface can sustain bound SPPs. When the separation between adjacent interfaces is comparable to or smaller than the decay length \hat{z} of the interface mode, interactions between SPPs give rise to coupled modes. In order to elucidate the general properties of coupled SPPs, we will focus on two specific three-layer systems of the geometry depicted in Fig. 2.5: Firstly, a thin metallic layer (I) sandwiched between two (infinitely) thick dielectric claddings (II, III), an insulator/metal/insulator (IMI) heterostructure, and secondly a thin dielectric core layer (I) sandwiched between two metallic claddings (II, III), a metal/insulator/metal (MIM) heterostructure.

Since we are here only interested in the lowest-order bound modes, we start with a general description of TM modes that are non-oscillatory in the z -direction normal to the interfaces using (2.8). For $z > a$, the field components are

$$H_y = A e^{i\beta x} e^{-k_3 z} \quad (2.22a)$$

$$E_x = iA \frac{1}{\omega \varepsilon_0 \varepsilon_3} k_3 e^{i\beta x} e^{-k_3 z} \quad (2.22b)$$

$$E_z = -A \frac{\beta}{\omega \varepsilon_0 \varepsilon_3} e^{i\beta x} e^{-k_3 z}, \quad (2.22c)$$

while for $z < -a$ we get

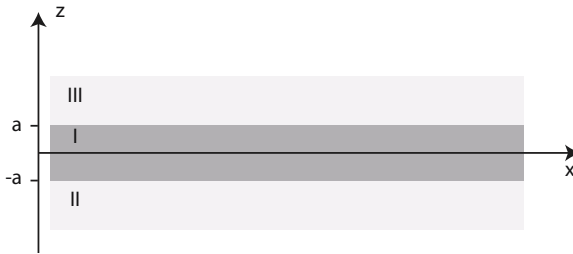


Figure 2.5. Geometry of a three-layer system consisting of a thin layer I sandwiched between two infinite half spaces II and III.

$$H_y = B e^{i\beta x} e^{k_2 z} \quad (2.23a)$$

$$E_x = -iB \frac{1}{\omega \varepsilon_0 \varepsilon_2} k_2 e^{i\beta x} e^{k_2 z} \quad (2.23b)$$

$$E_z = -B \frac{\beta}{\omega \varepsilon_0 \varepsilon_2} e^{i\beta x} e^{k_2 z}. \quad (2.23c)$$

Thus, we demand that the fields decay exponentially in the claddings (II) and (III). Note that for simplicity as before we denote the component of the wave vector perpendicular to the interfaces simply as $k_i \equiv k_{z,i}$.

In the core region $-a < z < a$, the modes localized at the bottom and top interface couple, yielding

$$H_y = C e^{i\beta x} e^{k_1 z} + D e^{i\beta x} e^{-k_1 z} \quad (2.24a)$$

$$E_x = -iC \frac{1}{\omega \varepsilon_0 \varepsilon_1} k_1 e^{i\beta x} e^{k_1 z} + iD \frac{1}{\omega \varepsilon_0 \varepsilon_1} k_1 e^{i\beta x} e^{-k_1 z} \quad (2.24b)$$

$$E_z = C \frac{\beta}{\omega \varepsilon_0 \varepsilon_1} e^{i\beta x} e^{k_1 z} + D \frac{\beta}{\omega \varepsilon_0 \varepsilon_1} e^{i\beta x} e^{-k_1 z}. \quad (2.24c)$$

The requirement of continuity of H_y and E_x leads to

$$A e^{-k_3 a} = C e^{k_1 a} + D e^{-k_1 a} \quad (2.25a)$$

$$\frac{A}{\varepsilon_3} k_3 e^{-k_3 a} = -\frac{C}{\varepsilon_1} k_1 e^{k_1 a} + \frac{D}{\varepsilon_1} k_1 e^{-k_1 a} \quad (2.25b)$$

at $z = a$ and

$$B e^{-k_2 a} = C e^{-k_1 a} + D e^{k_1 a} \quad (2.26a)$$

$$-\frac{B}{\varepsilon_2} k_2 e^{-k_2 a} = -\frac{C}{\varepsilon_1} k_1 e^{-k_1 a} + \frac{D}{\varepsilon_1} k_1 e^{k_1 a} \quad (2.26b)$$

at $z = -a$, a linear system of four coupled equations. H_y further has to fulfill the wave equation (2.8c) in the three distinct regions, via

$$k_i^2 = \beta^2 - k_0^2 \varepsilon_i \quad (2.27)$$

for $i = 1, 2, 3$. Solving this system of linear equations results in an implicit expression for the dispersion relation linking β and ω via

$$e^{-4k_1 a} = \frac{k_1/\varepsilon_1 + k_2/\varepsilon_2}{k_1/\varepsilon_1 - k_2/\varepsilon_2} \frac{k_1/\varepsilon_1 + k_3/\varepsilon_3}{k_1/\varepsilon_1 - k_3/\varepsilon_3}. \quad (2.28)$$

We note that for infinite thickness ($a \rightarrow \infty$), (2.28) reduces to (2.12), the equation of two uncoupled SPP at the respective interfaces.

We will from this point onwards consider the interesting special case where the sub- and the superstrates (II) and (III) are equal in terms of their dielectric response, i.e. $\varepsilon_2 = \varepsilon_3$ and thus $k_2 = k_3$. In this case, the dispersion relation (2.28) can be split into a pair of equations, namely

$$\tanh k_1 a = -\frac{k_2 \varepsilon_1}{k_1 \varepsilon_2} \quad (2.29a)$$

$$\tanh k_1 a = -\frac{k_1 \varepsilon_2}{k_2 \varepsilon_1}. \quad (2.29b)$$

It can be shown that equation (2.29a) describes modes of odd vector parity ($E_x(z)$ is odd, $H_y(z)$ and $E_z(z)$ are even functions), while (2.29b) describes modes of even vector parity ($E_x(z)$ is even function, $H_y(z)$ and $E_z(z)$ are odd).

The dispersion relations (2.29a, 2.29b) can now be applied to IMI and MIM structures to investigate the properties of the coupled SPP modes in these two systems. We first start with the IMI geometry - a thin metallic film of thickness $2a$ sandwiched between two insulating layers. In this case $\varepsilon_1 = \varepsilon_1(\omega)$ represents the dielectric function of the metal, and ε_2 the positive, real dielectric constant of the insulating sub- and superstrates. As an example, Fig. 2.6 shows the dispersion relations of the odd and even modes (2.29a, 2.29b) for an air/silver/air geometry for two different thicknesses of the silver thin film. For

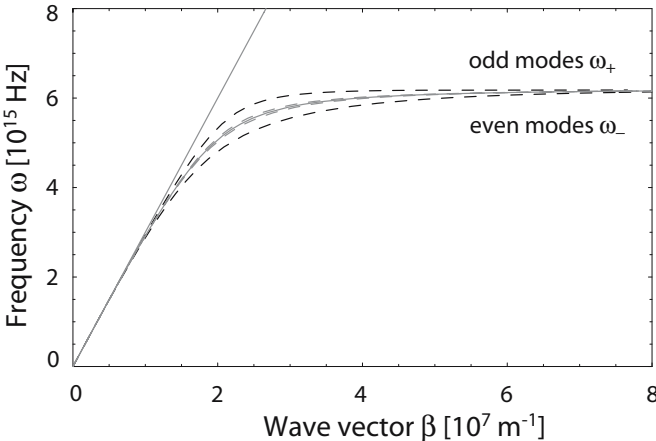


Figure 2.6. Dispersion relation of the coupled odd and even modes for an air/silver/air multilayer with a metal core of thickness 100 nm (dashed gray curves) and 50 nm (dashed black curves). Also shown is the dispersion of a single silver/air interface (gray curve). Silver is modeled as a Drude metal with negligible damping.

simplicity, here the dielectric function of silver is approximated via a Drude model with negligible damping ($\varepsilon(\omega)$ real and of the form (1.22)), so that $\text{Im}[\beta] = 0$.

As can be seen, the odd modes have frequencies ω_+ higher than the respective frequencies for a single interface SPP, and the even modes lower frequencies ω_- . For large wave vectors β (which are only achievable if $\text{Im}[\varepsilon(\omega)] = 0$), the limiting frequencies are

$$\omega_+ = \frac{\omega_p}{\sqrt{1 + \varepsilon_2}} \sqrt{1 + \frac{2\varepsilon_2 e^{-2\beta a}}{1 + \varepsilon_2}} \quad (2.30a)$$

$$\omega_- = \frac{\omega_p}{\sqrt{1 + \varepsilon_2}} \sqrt{1 - \frac{2\varepsilon_2 e^{-2\beta a}}{1 + \varepsilon_2}}. \quad (2.30b)$$

Odd modes have the interesting property that upon decreasing metal film thickness, the confinement of the coupled SPP to the metal film decreases as the mode evolves into a plane wave supported by the homogeneous dielectric environment. For real, absorptive metals described via a complex $\varepsilon(\omega)$, this implies a drastically increased SPP propagation length [Sarid, 1981]. These *long-ranging* SPPs will be further discussed in chapter 7. The even modes exhibit the opposite behavior - their confinement to the metal increases with decreasing metal film thickness, resulting in a reduction in propagation length.

Moving on to MIM geometries, we now set $\varepsilon_2 = \varepsilon_2(\omega)$ as the dielectric function of the metal and ε_1 as the dielectric constant of the insulating core in equations (2.29a, 2.29b). From an energy confinement point of view, the most interesting mode is the fundamental odd mode of the system, which does not exhibit a cut-off for vanishing core layer thickness [Prade et al., 1991]. Fig. 2.7 shows the dispersion relation of this mode for a silver/air/silver heterostructure. This time, the dielectric function $\varepsilon(\omega)$ was taken as a complex fit to the dielectric data of silver obtained by Johnson and Christy [Johnson and Christy, 1972]. Thus β does not go to infinity as the surface plasmon frequency is approached, but folds back and eventually crosses the light line, as for SPPs propagating at single interfaces.

It is apparent that large propagation constants β can be achieved even for excitation well below ω_{sp} , provided that the width of the dielectric core is chosen sufficiently small. The ability to access such large wave vectors and thus small penetration lengths \hat{z} into the metallic layers by adjusting the geometry indicates that localization effects that for a single interface can only be sustained at excitations near ω_{sp} , can for such MIM structures also be attained for excitation out in the the infrared. An analysis of various other MIM structures, for example concentric shells, has given similar results [Takahara et al., 1997]. Geometries amenable to easy fabrication such as triangular metal V-grooves

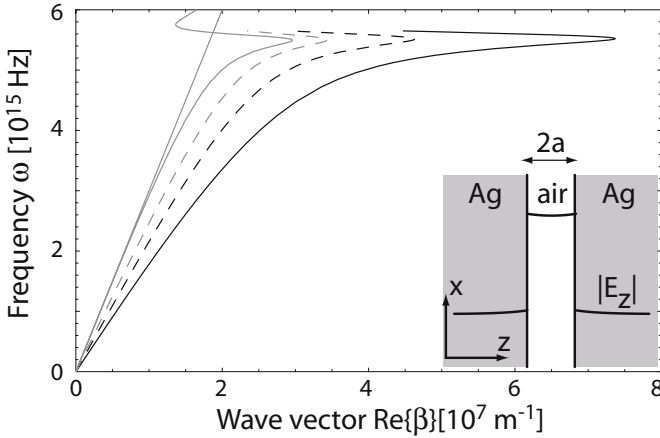


Figure 2.7. Dispersion relation of the fundamental coupled SPP modes of a silver/air/silver multilayer geometry for an air core of size 100 nm (broken gray curve), 50 nm (broken black curve), and 25 nm (continuous black curve). Also shown is the dispersion of a SPP at a single silver/air interface (gray curve) and the air light line (gray line).

on a flat metal surface have already shown great promise for applications in waveguiding, which will be presented in chapter 7.

We have limited our discussion of coupled SPPs in three-layer structures to the fundamental bound modes of the system, with a view on applications in waveguiding and confinement of electromagnetic energy. It is important to note that the family of modes supported by this geometry is much richer than described in this treatment. For example, for IMI structures, we have omitted a discussion of leaky modes, and MIM layers can also exhibit oscillatory modes for sufficient thickness of the dielectric core. Additionally, the coupling between SPPs at the two core/cladding interfaces changes significantly when the dielectric constants of the sub- and superstrates are different, so that $\epsilon_2 \neq \epsilon_3$, prohibiting phase-matching between the modes located at the two interfaces. A detailed treatment of these cases can be found in [Economou, 1969, Burke and Stegeman, 1986, Prade et al., 1991].

2.4 Energy Confinement and the Effective Mode Length

In chapter 5 we will see that using localized surface plasmons in metal nanoparticles, electromagnetic energy can be confined or squeezed into volumes smaller than the diffraction limit $(\lambda_0/2n)^3$, where $n = \sqrt{\epsilon}$ is the refractive index of the surrounding medium. This high confinement leads to a concomitant field enhancement and is of prime importance in plasmonics, enabling a great variety of applications in optical sensing, as will be discussed in chapter 9. In the essentially one-dimensional cases of single interfaces and

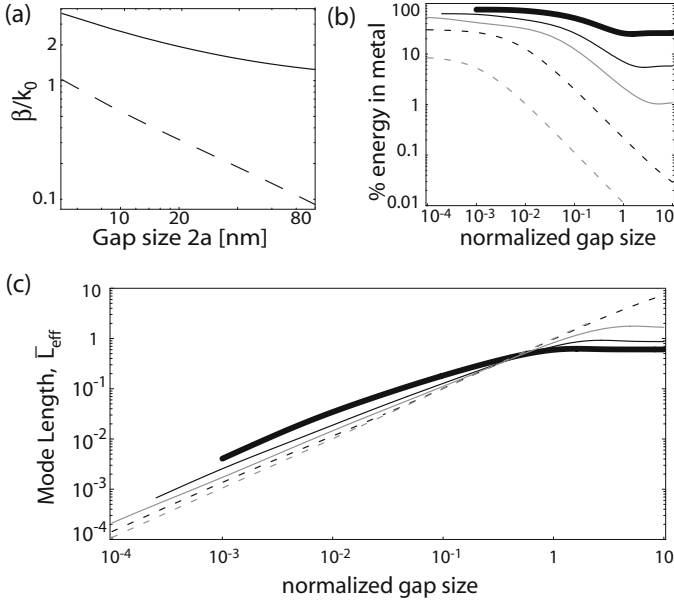


Figure 2.8. Energy confinement in a gold/air/gold MIM structure. (a) Real (solid curve) and imaginary (dashed curve) part of the normalized propagation constant β versus gap size at $\lambda_0 = 850\text{nm}$. (b) Fraction of electric field energy residing inside the metallic half spaces as a function of normalized gap size for excitation at $\lambda_0 = 600\text{ nm}$ (thick curve), 850nm (black curve), $1.5\ \mu\text{m}$ (gray curve), $10\ \mu\text{m}$ (broken black curve), and $100\ \mu\text{m}$ (broken gray curve). (c) Effective mode length L_{eff} normalized to free-space wavelength λ_0 as a function of gap size. Adapted from [Maier, 2006b].

multilayer structures presented above that support propagating SPPs, energy localization below the diffraction limit perpendicular to the interface(s) is also possible. We have already hinted at this phenomenon when stating that the field decay length \hat{z} in the dielectric layers can be significantly smaller than λ_0/n .

However, care must be taken when quantifying energy confinement, since a sub-wavelength field decay length \hat{z} on the dielectric side of the interface implies that a significant amount of the total electric field energy of the SPP mode resides inside the metal. This energy must be taken into account using (1.38) when calculating the spatial distribution of the electric energy density, since for the quantification of the strength of interactions between light and matter (e.g. a molecule placed into the field), the field strength per unit energy (i.e., single photon) is of importance.

Taking a gold/air/gold MIM heterostructure as an example, Fig. 2.8(a) shows the evolution of both the real and imaginary parts of the propagation constant β of the fundamental SPP mode with varying gap size for excitation at a free space wavelength of $\lambda_0 = 850\text{ nm}$, calculated using Drude fits to the dielectric

function of gold [Johnson and Christy, 1972, Ordal et al., 1983]. Both parts increase with decreasing gap size, since the mode is becoming more electron-plasma in character, suggesting that the electromagnetic energy is residing increasingly in the metal half-spaces. A plot of the fractional amount of the electric field energy inside the metal regions is shown in Fig. 2.8(b) for excitation at wavelengths $\lambda_0 = 600 \text{ nm}$, 850 nm , $1.5 \mu\text{m}$, $10 \mu\text{m}$, and $100 \mu\text{m}$ ($= 3 \text{ THz}$). For a gap of 20 nm for example, at $\lambda_0 = 850 \text{ nm}$ this fraction already reaches 40%. Note that the gap size is normalized to the respective free space wavelength. It is apparent that along with the increased localization of the field to the gold/air interface, either via small gap sizes or excitation closer to ω_{sp} , comes a shift of the energy into the metal regions.

In order to get a better handle on the consequences of increasing fractions of the total energy of the mode entering the metallic cladding upon decreasing size of the dielectric gap, we can define in analogy to the effective mode *volume* V_{eff} used to quantify the strength of light-matter interactions in cavity quantum electrodynamics [Andreani et al., 1999] an effective mode *length* L_{eff} , with

$$L_{\text{eff}}(z_0)u_{\text{eff}}(z_0) = \int u_{\text{eff}}(z)dz. \quad (2.31)$$

$u_{\text{eff}}(z_0)$ represents the electric field energy density at a position z_0 of interest within the air core (e.g. the location of an emitter). In this one-dimensional picture, the effective mode length is therefore given as the ratio of the total energy of the SPP mode divided by the energy density (energy per unit length) at the position of interest, which is often taken as the position of highest field. In a quantized picture for normalized total energy, the inverse of the effective mode length thus quantifies the field strength per single SPP excitation. More details can be found in [Maier, 2006b].

A determination of the effective mode length of MIM structures allows an examination how the electric field strength per SPP excitation in the air gap scales as a function of the gap size. Fig. 2.8(c) shows the variation of L_{eff} (normalized to the free-space wavelength λ_0) with normalized gap size. z_0 is taken to be at the air side of the air/gold boundary, where the electric field strength is maximum. The mode lengths drop well below $\lambda_0/2$, demonstrating that plasmonic metal structures can indeed sustain *effective* as well as *physical* mode lengths below the diffraction limit of light. The trend in L_{eff} with gap size tends to scale with the physical extent of the air gap. For large normalized gap sizes and low frequencies, this is due to the delocalized nature of the surface plasmon, leading to smaller mode lengths for excitation closer to the surface plasmon frequency ω_{sp} for the same normalized gap size.

As the gap size is reduced to a point where the dispersion curve of the SPP mode turns over (see Fig. 2.7) and energy begins to enter the metallic half spaces, the continued reduction in mode length is due to an increase in field

localization to the metal-air interface. In this regime, excitations with lower frequencies show smaller mode lengths for the same normalized gap size than excitations closer to the plasmon resonance, due to the fact that more energy resides inside the metal for the latter. We note that for very small gaps with $2a < 2$ nm, the effects of local fields due to unscreened surface electrons become important [Larkin et al., 2004], leading to a further decrease in L_{eff} . This cannot be captured using the dielectric function approach.

To summarize, we see that despite the penetration of a significant amount of energy of a SPP mode into the conducting medium (for excitation near ω_{sp} or in small gap structures), the associated large propagation constants β ensure that the effective extent of the mode perpendicular to the interface(s) drops well below the diffraction limit.



<http://www.springer.com/978-0-387-33150-8>

Plasmonics: Fundamentals and Applications

Maier, S.A.

2007, XXVI, 224 p., Hardcover

ISBN: 978-0-387-33150-8